J Mater Sci (2016) 51:2529–2539
DOI 10.1007/s10853-015-9565-0

Microstructural evolution in 316LN austenitic stainless steel during solidification process under different cooling rates

Congfeng Wu[1] · Shilei Li[1] · Changhua Zhang[1] · Xitao Wang[2]

Received: 23 August 2015 / Accepted: 3 November 2015 / Published online: 20 November 2015

Abstract The solidification sequence and microstructure evolution during solidification process of two 316LN stainless steels with different compositions under different cooling rates were in situ observed with confocal scanning laser microscope. The results show that 316LN solidifies with primary austenite or primary δ ferrite when the cooling rate is small in the range of conventional casting process, depending on the value of Cr_{eq}/Ni_{eq} which are calculated by Hammar and Svensson equations. As the cooling rate increases in the range of 0–100 °C s^{-1}, the solidification sequences do not change, but both the dendrite arm spacing and the mean free path between δ ferrite decrease. In addition, concomitant with the variations of chemical composition in δ ferrite and austenite are the shape transformation of interdendritic δ ferrite from island-like to lacy-like and the coarsening of dendrite δ ferrite with cooling rate increasing. The mechanism of three-phase reaction in 316LN with different compositions, i.e., eutectic reaction or peritectic reaction, was analyzed. The bigger diffusivities of Cr and Ni in primary δ ferrite than that in primary austenite and the positions of alloys in phase diagram were thought to be the main reasons for the difference in type of the reaction.

✉ Xitao Wang
xtwang@ustb.edu.cn

Congfeng Wu
wucongfeng1986@gmail.com

Shilei Li
dylishilei@gmail.com

Changhua Zhang
1269963444@qq.com

[1] State Key Laboratory for Advanced Metals and Materials, University of Science and Technology Beijing, Beijing 100083, People's Republic of China

[2] Collaborative Innovation Center of Steel Technology, University of Science and Technology Beijing, Beijing 100083, People's Republic of China

Introduction

The solidification microstructure of austenitic stainless steel has always been the interest of researches in academia and industry because it determines the castability, weldability, hot workability, mechanical properties, and corrosion resistance [1–4]. In austenitic stainless steels, a three-phase reaction region (L + δ + γ), which can be either eutectic or peritectic, exists for compositions of over 15 wt% Cr and 10 wt% Ni according to the Fe–Cr–Ni ternary phase diagram [5, 6]. Therefore, the solidification microstructure, which mainly depends on both composition and cooling rate, is complex as a result of the complicated three-phase reaction [5, 7]. Suutala [8] investigated the solidification conditions on solidifying sequence of a range of AISI 300 series steels by autogenous gas tungsten arc (GTA) welding and concluded that the composition was of primary importance while the cooling rate was only of secondary importance. However, a given austenitic stainless steel with composition passing through the Cr-rich part of the three-phase region can solidify with primary δ ferrite or primary γ phase under different cooling rates [8–10]. The different solidifying sequences would result in change of elements redistribution path, and thus may alter the type of three-phase reaction and the solidification microstructure. Ma et al. [11] and Fu et al. [12, 13] investigated the detailed microstructural evolution process in directional solidified 304 austenitic stainless steel under estimated cooling rates of 3.3, 1, and 4 °C s^{-1}, respectively. They concluded that eutectic reaction

Table 1 Chemical compositions of AISI 316LN stainless steel

Alloy	C	N	Si	Mn	Cr	Ni	Mo	P	S	Fe
316LN-1	0.0076	0.13	0.25	1.30	17.86	12.72	2.80	0.0052	0.0046	Bal.
316LN-2	0.0043	0.11	0.17	1.31	17.00	11.24	2.32	0.0053	0.0046	Bal.

($L \rightarrow \gamma + \delta$) which resulted in the formation of coupled structure occurred among the dendrite arms after primary δ ferrite precipitated from liquid. Liang et al. [14] observed a different phenomenon in 301 austenitic stainless steel at cooling rates of 4–25 °C s^{-1} under non-directional solidification condition using differential thermal analysis (DTA). They found that peritectic reaction and eutectic reaction coexisted in the microstructure of the sample cooled at 25 °C s^{-1}. In addition, many other researchers [15–17] investigated the solidification microstructure of various austenitic stainless steels by sorts of welding methods which have much higher cooling rate than casting and directional solidification. However, the three-phase reaction mechanism is still unclear and it was not directly observed in the above-mentioned literatures owing to the limitations of test method. Confocal scanning laser microscope (CSLM) enables the in situ observation of phase transformation at high temperature, as shown in references [18–20]. Huang et al. [19] and McDonald et al. [20] observed the δ/γ interface and microstructure evolution during the peritectic reaction at a cooling rate of 0.05 °C s^{-1} and constant undercooling degree, respectively. Nevertheless, the effect of larger cooling rate, which may be confronted in many types of conventional casting processes, on the microstructure evolution has not been studied, nor has been the in situ observation.

AISI 316LN steel, a type of nitrogen-alloyed ultralow carbon (<0.02 wt%) stainless steel, is used as the material of main pipelines in AP1000 pressurized water reactor (PWR) which is about to commercially serve in China. The pipes are manufactured by integral hot forging and the ingots for hot forging are obtained by mold casting or electro slag remelting (ESR) which has typical cooling rates of 0–100 °C s^{-1} [17]. Therefore, in this regard, the studies of phase transformation in 316LN during solidification under different cooling rates would be of interest.

In this paper, two 316LN stainless steels with different compositions were used to investigate their solidification sequence and microstructure evolution. The three-phase reaction was in situ observed in CSLM under different cooling rates and the variation of chemical composition in different phases was discussed.

Experimental

Two ingots of AISI 316LN stainless steel with different values of Cr_{eq}/Ni_{eq} were produced by vacuum induction furnace (VIF) and the casting was carried out at a constant superheat of 50 °C in a cast-iron ingot mold. The ingots were forged at 1200 °C and then solution treated at 1100 °C for 4 h. The chemical compositions are given in Table 1.

The cooling rate of this type of mold casting was estimated to be ~2.00 °C s^{-1} according to the relationship of secondary dendrite arm spacing (SDAS, λ_2) to cooling rate (ε): $\lambda_2 = 68 \times (\varepsilon)^{-0.45}$ [17, 21, 22]. In order to directly observe the microstructural evolution under different cooling rates, a CSLM (VL2000DX, Lasertec, Japan) was used. The principle of this equipment is described in many literatures [19, 20]. The disc samples with dimensions of φ7 × 3 mm for observation were machined from the solution-treated materials, and then they were mechanically polished with diamond paste. Subsequently, they were put in an alumina crucible which was installed into a furnace at the focal point of the sample chamber. After the chamber was filled with argon, the samples were heated to the melting points and kept for 60 s, and next they were cooled down to 1100 °C with cooling rates of 2, 10, and 100 °C s^{-1}, respectively (see Fig. 1).

After the samples were cooled down to room temperature, they were prepared by conventional process for metallographic observation. The etchant solution contains 0.5 g $K_2S_2O_5$, 20.0 g NH_4FHF, and 100 ml distilled water (Beraha's etchant modified by Lichtenegger [16]), whose pH value was maintained at about 2.5 by addition of NH_4OH or HNO_3. Electron probe microanalyzer (EPMA) (JEOL JXA-8230, Japan) was employed to characterize the variation of chemical composition. The volume fractions of primary δ ferrite and primary austenite during in situ observation were measured by image analysis using software of Image Tool Version 3.0.

Results

As-cast microstructure of mold casting ingots

The as-cast microstructures of mold casting 316LN-1 and 316LN-2 are shown in Fig. 2. Beraha's etchant makes Cr-rich areas show light color contrast and Cr-depleted areas darker (blue or green) color contrast [16]. In other words, ferrite remains unaffected showing as whiteness, while austenite exhibits a range of colors depending on its Cr concentration. Therefore, the white island-like phase which lies in interdendritic areas in Fig. 2a is ferrite. This indicates that austenite is primary phase and δ ferrite forms at

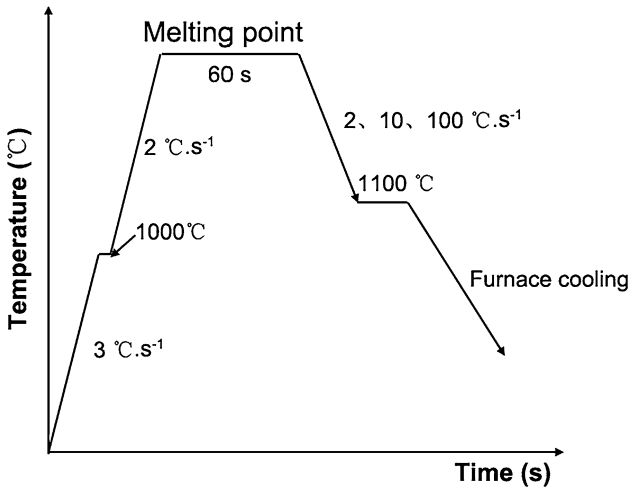

Fig. 1 Schematic of heating and cooling curves of specimens during in situ observation

the final stage of solidification in alloy 316LN-1. While in 316LN-2, skeletal δ ferrite exists in dendrite branches (see Fig. 2b), which means that δ ferrite precipitates from liquid firstly and austenite forms later. The solidification behaviors during mold casting process may approximate the equilibrium process because the cooling rate of ~2 °C s^{-1} is relatively small in the range of conventional casting processes. When the cooling rate becomes high enough, the solidification behavior will deviate from the equilibrium process, and different solidification microstructures may appear.

Solidified microstructures of 316LN under different cooling rates

Figure 3 presents the solidified microstructures of alloy 316LN-1 under different cooling rates. When the steel was cooled at 2 °C s^{-1}, δ ferrite exists in both interdendritic areas and dendrite branches, as shown in Fig. 3a and b. However, the interdendritic δ ferrite is predominant. The dendrite branch shows light color contrast which means that its Cr concentration is higher than adjacent area (see Fig. 3b). This characteristic is not consistent with the feature of elements segregation in Fig. 2a, which may be associated with the fact that the steel was not fully melted owing to the limitation of the equipment as the temperature reached the peak point (see Fig. 4). The unmelted parts, which are richer in Cr element as a result of redistribution of elements during the reaction of $L + \delta + \gamma \rightarrow L + \gamma$ on heating, become dendrite branches as the solidification goes on. When the temperature decreases, the dendritic δ ferrite appears owing to the higher Cr concentration.

As the cooling rate increases, δ ferrite still mainly forms in interdendritic areas which can be seen in Fig. 3c–f, but the amount of dendritic δ ferrite is reduced. The shape of ferrite changes from island-like to lacy-like with increasing of cooling rate due to the shortening of diffusion path [23]. Furthermore, both the dendrite arm spacing (DAS) and the mean free path between δ ferrite decrease owing to the inhibition of element redistribution and quicker heat rejection under higher undercooling [17]. Overall, in view of the larger variances of content changes at 10 °C s^{-1}, contents of Cr and Mo can be thought to decrease slightly in both δ ferrite and γ phase while Ni increases in γ phase and decreases in δ ferrite in a small scale with the increasing of cooling rate, as shown in Fig. 5. The larger variances at 10 °C s^{-1} may be caused by the bigger scattering of measurement points.

The solidified microstructures of alloy 316LN-2 under different cooling rates are shown in Fig. 6. δ ferrite precipitates in dendrite branches under cooling rate of 2 °C s^{-1}, and a coupled growth microstructure of δ + γ was observed when cooled at 10 and 100 °C s^{-1}. In particular, δ ferrite becomes coarser due to the suppression of time for solid-state transformation from δ to γ when cooling rate increases. In pace with this coarsening

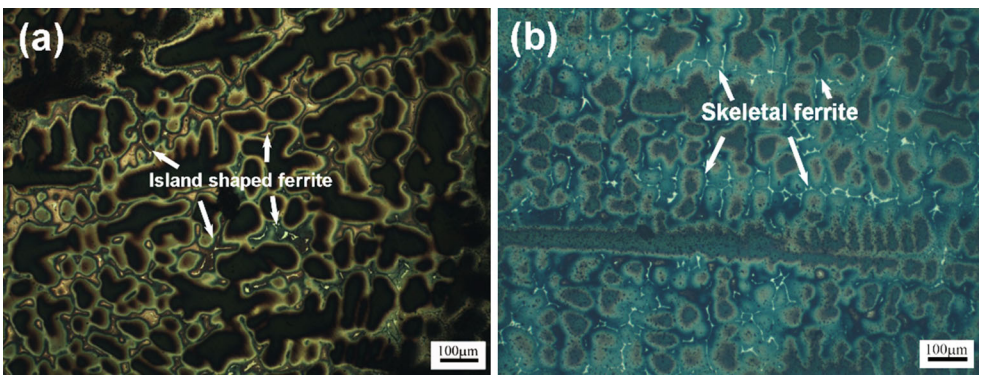

Fig. 2 As-cast microstructure of 316LN stainless steel: **a** 316LN-1, **b** 316LN-2

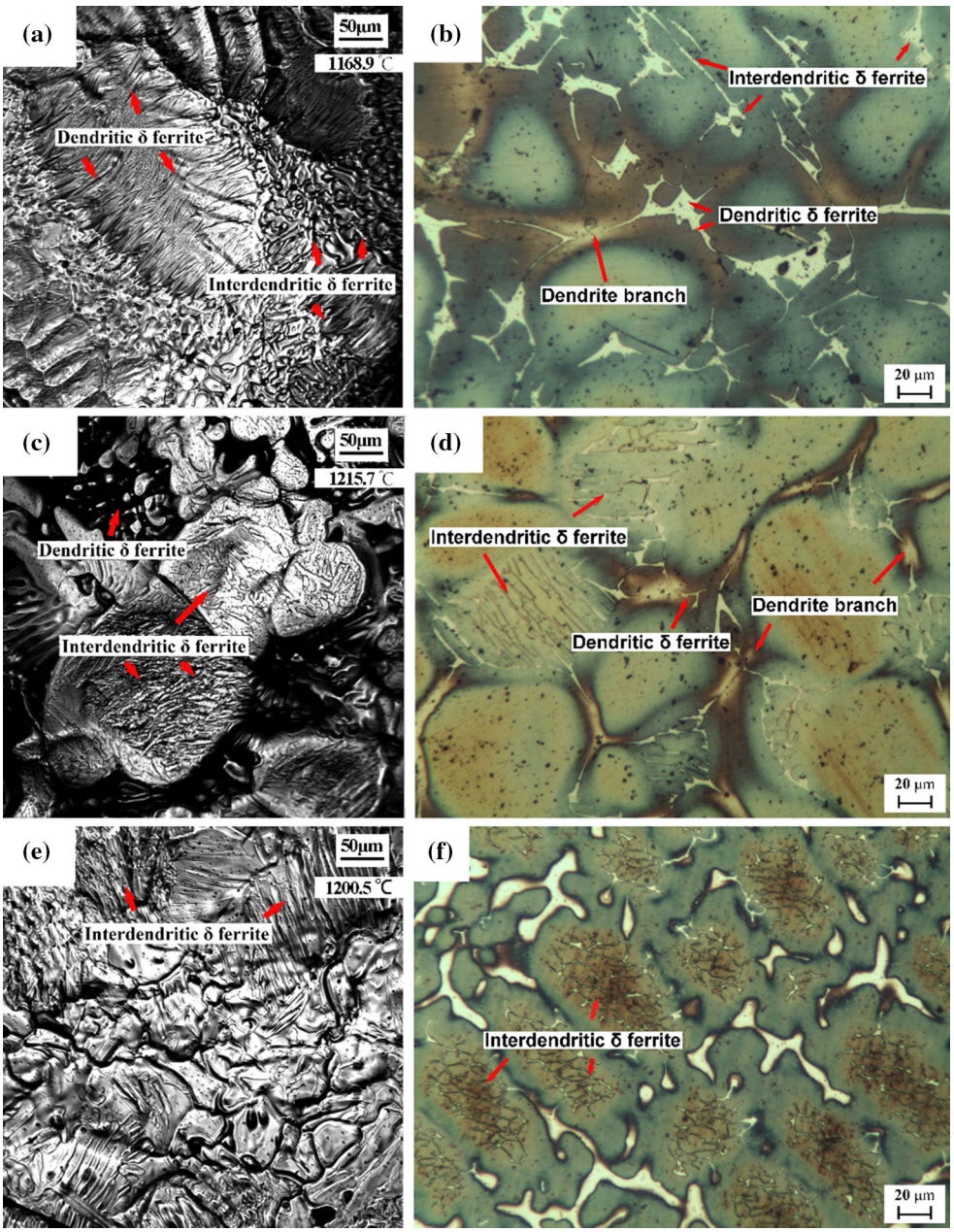

Fig. 3 In situ observation and metallurgical micrographs of the solidified microstructure in alloy 316LN-1 under different cooling rates. **a**, **b** 2 °C s^{-1}; **c**, **d** 10 °C s^{-1}; **e**, **f** 100 °C s^{-1}

behavior, the element contents in δ ferrite and γ phase change regularly, as shown in Fig. 7. Cr and Mo increase and Ni decreases in δ ferrite, while in γ phase they change in a reverse direction with the increasing of cooling rate. This phenomenon is thought to be caused by the inhibition of element diffusion during δ → γ transformation as the cooling rate increases [11, 17]. It can be seen that the contents change trend in 316LN-2 is more obvious than that in 316LN-1 and their variation trend of Cr and Mo in δ ferrite is opposite. This can be understood based on that the δ ferrite in 316LN-1 generates through the reaction of L → δ + γ at the final stage of solidification, as will be discussed in next section. As the cooling rate increases, the amount of remaining liquid between primary austenite decreases and therefore the amount of δ ferrite decreases. Thus, the contents of Cr and Mo in δ ferrite decrease, while they increase in 316LN-2 because its δ ferrite is primary phase and the outward diffusion rate of Cr and Mo from δ ferrite was suppressed by increasing cooling rate.

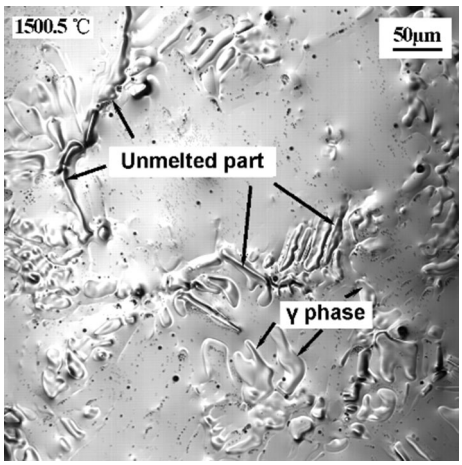

Fig. 4 High temperature microstructure of alloy 316LN-1

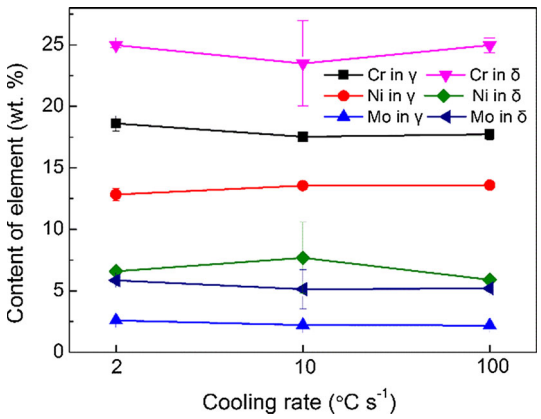

Fig. 5 Effect of cooling rate on the variations of composition in 316LN-1

Discussion

Solidification mode

From the above results, the precipitation sequences and morphologies of ferrite can vary, depending on the composition and cooling rate. This can be illustrated by the concept of solidification mode. The solidification mode of austenitic stainless steel can be divided into four types according to the value of Cr_{eq}/Ni_{eq} [8, 24]:

F mode : $L \rightarrow L + \delta \rightarrow \delta \rightarrow \delta + \gamma$	$Cr_{eq}/Ni_{eq} > 2.00$
FA mode : $L \rightarrow L + \delta \rightarrow L + \delta + \gamma \rightarrow \delta + \gamma \rightarrow \gamma$	$1.50 < Cr_{eq}/Ni_{eq} < 2.00$
AF mode : $L \rightarrow L + \gamma \rightarrow L + \delta + \gamma \rightarrow \gamma + \delta \rightarrow \gamma$	$1.37 < Cr_{eq}/Ni_{eq} < 1.50$
A mode : $L \rightarrow L + \gamma \rightarrow \gamma$	$Cr_{eq}/Ni_{eq} < 1.37$

where A and F refer to austenite and ferrite, respectively. The values of Cr_{eq} and Ni_{eq} can be calculated using the following Hammar and Svensson equations [24]:

$$Cr_{eq} = Cr + 1.37Mo + 1.5Si + 2Nb + 3Ti \quad (1)$$

$$Ni_{eq} = Ni + 22C + 14.2N + 0.31Mn + Cu \quad (2)$$

For the alloys 316LN-1 and 316LN-2 studied here, the ratios of Cr_{eq} to Ni_{eq} equal 1.47 and 1.55, respectively. Hence, alloy 316LN-1 falls into AF mode while alloy 316LN-2 follows FA mode. This indicates that austenite is the primary phase in 316LN-1 and the precipitation of δ ferrite occurs first in 316LN-2, then three-phase reaction ($L + \delta + \gamma$) comes about at the terminal stage of solidification in both alloys. Subsequently, solid-state transformation of $\delta \rightarrow \gamma$ continues below solidus lines [12, 25]. Therefore, the results predicted by Hammar and Svensson equations work fairly concordant with the solidified microstructure of mold casting in Figs. 3 and 6.

In respect of the effect of cooling rate on the solidification mode, the results in Figs. 3 and 6 show that this effect can be almost ignored in the range of 0–100 °C s^{-1}, except that a small region of primary ferrite which co-existed with primary austenite was found in alloy 316LN-2 when it was cooled at 100 °C s^{-1} (see Fig. 8). That is to say, the solidification mode of FA type in 316LN may change to AF mode if the cooling rate is greater than 100 °C s^{-1}. In this case, the available time for segregation in front of dendrite tip becomes less on account of the high cooling rate [17]. Consequently, the dendritic growth transforms into cellular growth, which results in the achievement of critical value of undercooling degree for metastable austenite formation [8, 17, 26]. While in alloy 316LN-1, its solidification mode may change to A mode under large enough undercooling conditions because the precipitation of interdendritic ferrite will be suppressed by high cooling rate, whereas it does not occur under current conditions.

Solidification process of 316LN

Figure 9 presents some representative micrographs of phase formation during in situ observation in alloy 316LN-1 when it was cooled at 2 °C s^{-1}. Based on AF solidification mode, the solidification process can be described as below: when the melt undercooling degree reached a

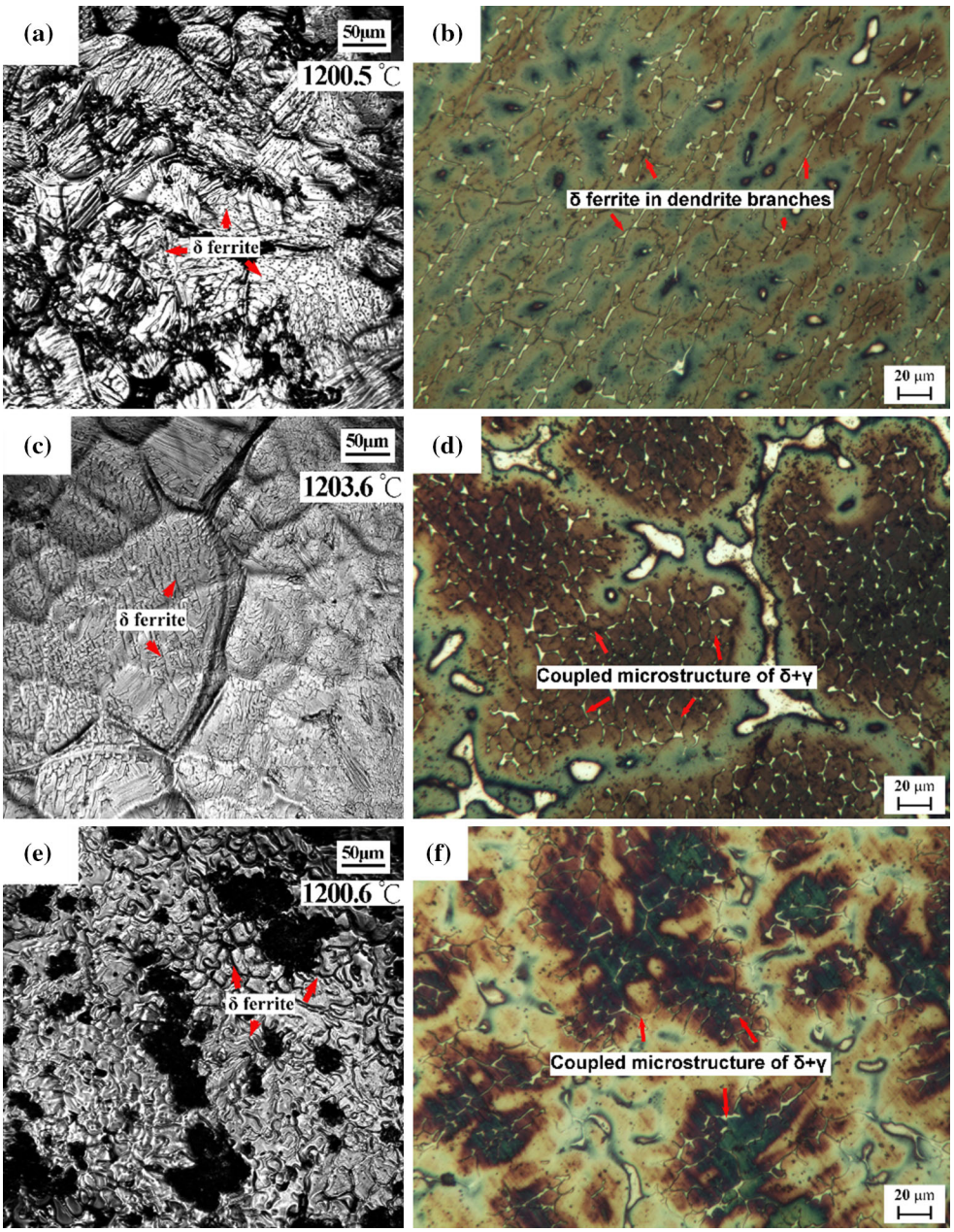

Fig. 6 In situ observation and metallurgical micrographs of solidified microstructure in alloy 316LN-2 under different cooling rates. **a**, **b** 2 °C s^{-1}; **c**, **d** 10 °C s^{-1}; **e**, **f** 100 °C s^{-1}

critical value, primary γ phase appeared in liquid and grew in the form of dendrite with the temperature decreasing (see Fig. 9a, b). During this process, Cr and Mo were rejected to liquid [16] and the austenite liquidus line was also lowered down, which both favored for the formation of δ ferrite. Subsequently, a eutectic reaction of $L \rightarrow \gamma + \delta$ was observed among the primary austenite dendrite when the temperature dropped to 1464.9 °C (see Fig. 9c). As temperature reached 1349.3 °C, the liquid phase disappeared and the solid-state transformation of $\delta \rightarrow \gamma$ occurred. As discussed in the above section, the solidification mode and δ ferrite's distribution in 316LN-1 did not change as the cooling rate increased, so did the solidification process. Figure 10 shows the phases evolution during in situ observation in 316LN-1 at 100 °C s^{-1}, and we can see that the characteristics of phases formation are similar to that in Fig. 9 except the corresponding time and temperature.

In alloy 316LN-2, different features of phase evolution were observed when it was also cooled at 2 °C s^{-1}. Figure 11a and b show that primary δ ferrites precipitated along impurities and grew into liquid with the temperature

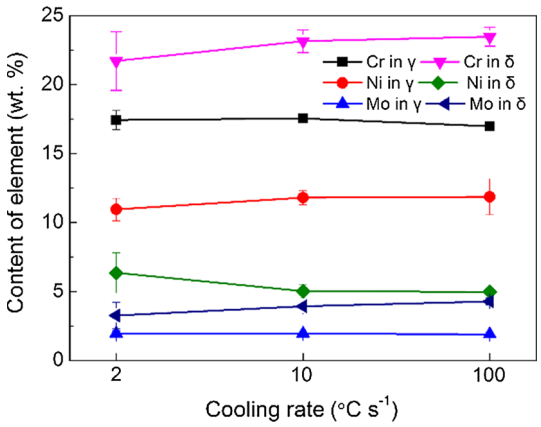

Fig. 7 Effect of cooling rate on the variations of chemical composition in alloy 316LN-2

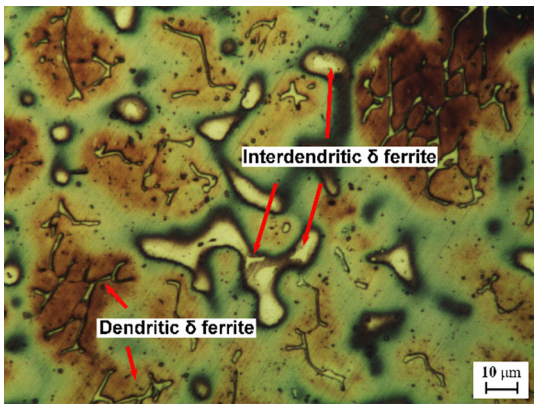

Fig. 8 Solidified microstructure of alloy 316LN-2 cooled at rate of 100 °C s^{-1}

decreasing. As this process went on, Ni was partitioned to the remaining liquid while Cr and Mo were absorbed into δ ferrites [13]. Subsequently, γ phase formed at the boundaries of δ ferrite and liquid through the peritectic reaction of L + δ → γ, as shown in Fig. 11c, d. At temperature of 1377.90 °C, liquid phase disappeared and the solid-state transformation from δ ferrite to austenite occurred (see Fig. 11e). Concurrently, Cr was rejected and Ni was accepted by austenite, which resulted in the increasing of austenite's relative stability. However, as a result of the limitation of elements diffusion on cooling, the transformation from δ ferrite to austenite was uncomplete, and therefore, skeletal ferrite, which is enriched in Cr and Mo while depleted in Ni, was retained in the core area of dendrites (see Fig. 11f). Particularly, it should be mentioned that the impurities were mostly retained around the boundaries of δ ferrite and interdendritic austenite because the solidifying interfaces can push the impurities if the critical radius for pushing or engulfment transition of nonmetallic is larger than inclusion size [27, 28]. Liang et al. [29] also observed this phenomenon in their work and thought that δ ferrite can absorb the inclusions moving near the δ-L interface.

The biggest difference between the solidification process of alloy 316LN-1 and 316LN-2 is the precipitation sequence of ferrite and austenite, which has been discussed by many authors [16, 17, 30, 31]. In addition, the alloys behaved in different types of reaction in three-phase region, i.e., eutectic reaction in 316LN-1 and peritectic reaction in 316LN-2, as shown in Figs. 9c and 11c. Figure 12 shows the equilibrium phase diagrams calculated by JMatPro software (version 6.1) and illustrates the positions of 316LN-1 and 316LN-2 in vertical section of Fe–Cr–Ni ternary diagram at constant Fe content. Based on the above results of observation and analysis, it is certain that the melt undercooling degree before solidification process which started did not reach the difference between the liquidus temperature of austenite T_L^{γ} and the eutectic trough temperature (T_E, indicated by point E in Fig. 12b) in 316LN-1 and that between T_L^{δ} and T_E in 316LN-2. Therefore, when the critical undercooling degree for austenite nucleation (ΔT_{γ}) in 316LN-1 and that for δ ferrite nucleation (ΔT_{δ}) in 316LN-2 were reached, austenite or δ ferrite firstly precipitated from liquid phase, respectively. However, the volume fraction of primary δ ferrite ($\varphi_{\delta} = 85.4$ % in Fig. 9c) in 316LN-2 was more than that of primary austenite ($\varphi_{\gamma} = 50.2$ % in Fig. 11c) in 316LN-1, because of the about 100 times larger diffusivities of Cr and Ni in ferrite than that in austenite [32] and the more nucleation sites in 316LN-2. Consequently, the remaining liquid phase in 316LN-1 when three-phase reaction began was more than that in 316LN-2. Moreover, the difference between T_L^{δ} and the temperature of three-phase reaction beginning (T_t) in 316LN-2 was calculated to be 29 °C, which is much larger than that between T_L^{γ} and T_t, 5.1 °C, in 316LN-1. Therefore, the bigger temperature drop and less remaining liquid phase in 316LN-2 facilitated the peritectic reaction owing to the more amount of primary phase and shorter diffusion distance between δ and L. While in alloy 316LN-1, the longer diffusion distance between primary γ and L, combined with the fact that the cooling line of 316LN-1 in the ternary phase diagram is nearer to eutectic trough than that of 316LN-2 (austenite and δ ferrite almost precipitate simultaneously in 316LN-1 according to Fig. 12a), prompted the eutectic reaction.

While cooling rate increases, the type of three-phase reaction in 316LN-1 does not change. However, under the conditions of 10 and 100 °C s^{-1}, the peritectic reaction transforms into eutectic reaction in 316LN-2, which results in the appearance of a coupled growth microstructure of δ + γ. The main reason for this transformation is that the melt undercooling degrees at the beginning of solidification become higher than the difference in values between T_L^{δ} and

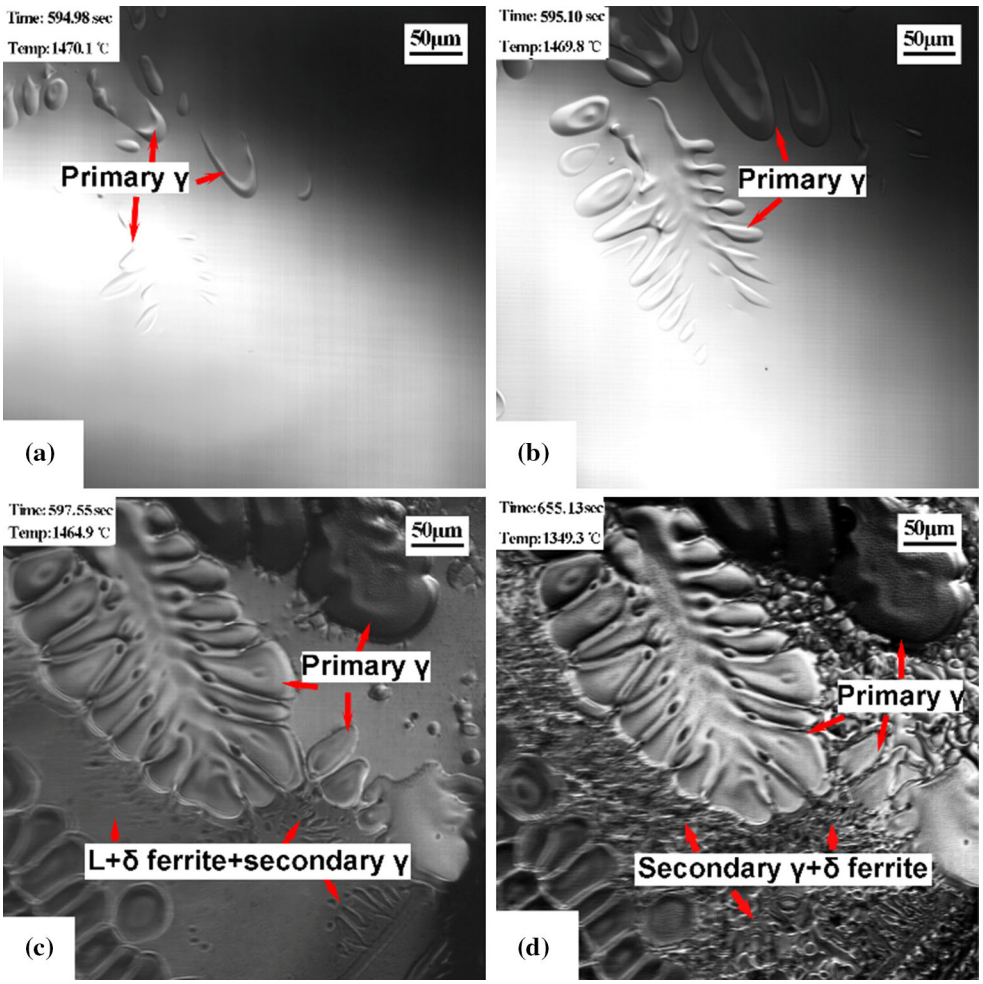

Fig. 9 In situ observation of phase formation during solidification in alloy 316LN-1 at 2 °C s^{-1}. **a**, **b** Primary austenite appeared and grew in liquid; **c** eutectic reaction occurred among the dendrite; **d** liquid disappeared at 1349.3 °C

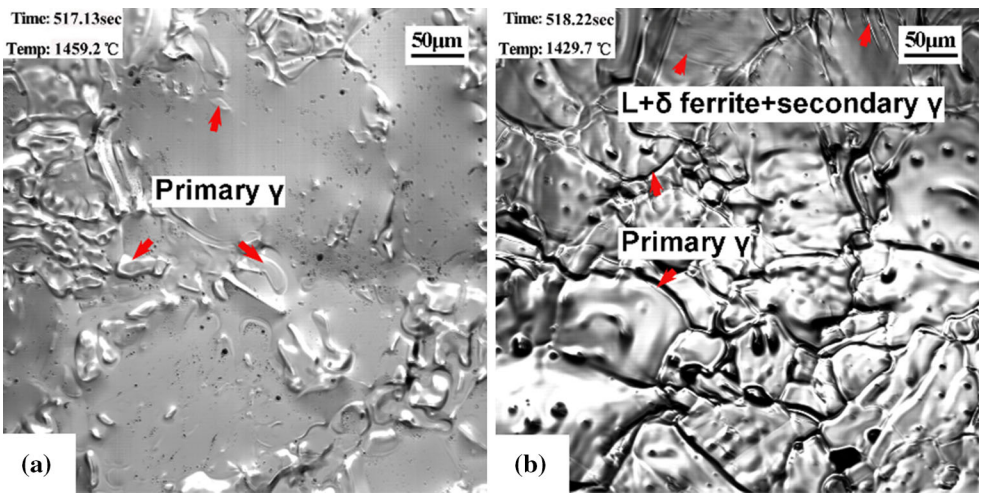

Fig. 10 In situ observation of phase formation during solidification in alloy 316LN-1 at 100 °C s^{-1}. **a** Primary austenite grew in liquid; **b** eutectic reaction occurred among the dendrite

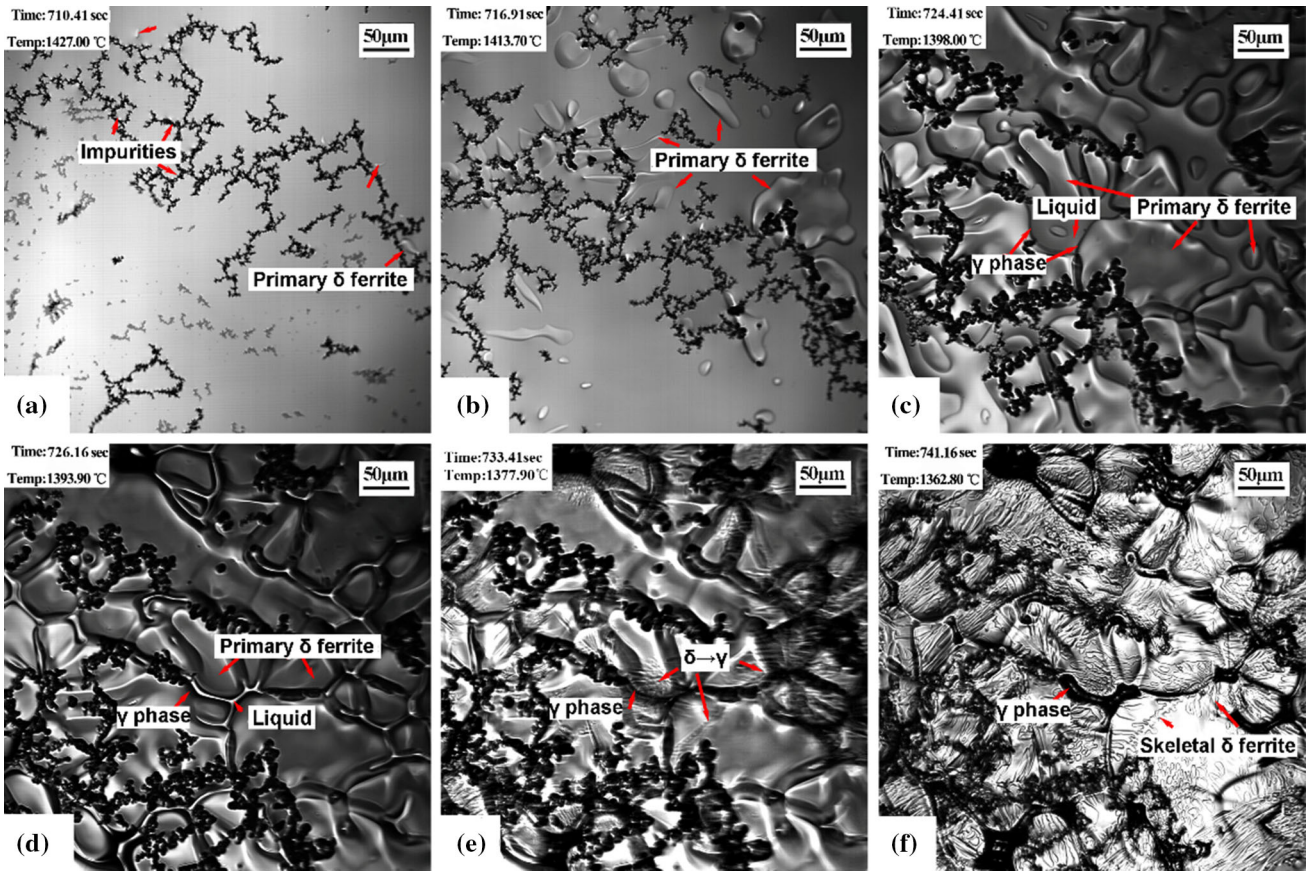

Fig. 11 In situ observation of phase formation during solidification in alloy 316LN-2 at 2 °C s^{-1}. **a**, **b** Primary ferrite appeared and grew in liquid; **c**, **d** peritectic reaction occurred at ferrite/liquid boundaries; **e** liquid disappeared at 1377.9 °C and solid state transformation occurred; **f** skeletal ferrite was retained in core area of dendrites

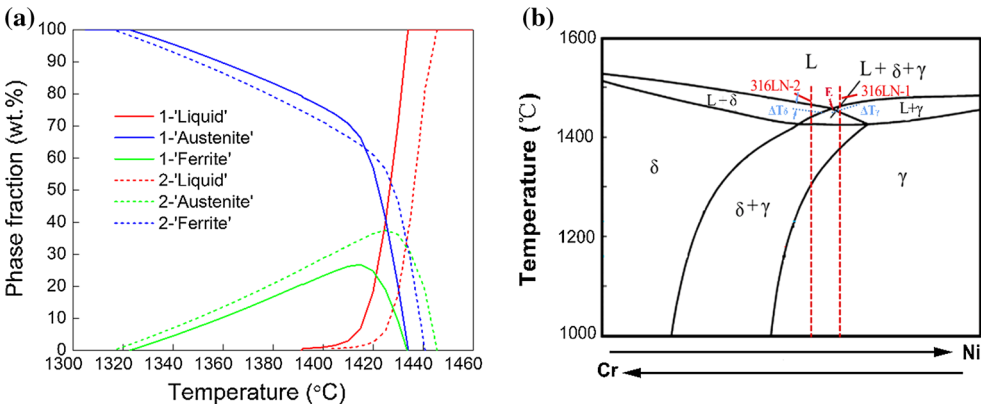

Fig. 12 Equilibrium phase diagram calculated by JMatPro software (**a**) and vertical section of Fe–Cr–Ni ternary diagram at constant Fe (**b**)

T_E. Therefore, δ + γ microstructure formed directly without the occurrence of primary δ ferrite, as shown in Fig. 13.

Conclusions

In situ observation with CSLM and color metallographic method were carried out in two 316LN stainless steels with different compositions in order to investigate their solidification sequence and microstructure evolution during solidification process. The effects of cooling rate on variations of microstructure and chemical composition were also studied. These experimental investigations allow the following conclusions to be reached:

(1) During mold casting process, alloy 316LN-1 follows the solidifying path of AF solidification mode, while 316LN-2 solidifies in FA mode. Both the results are

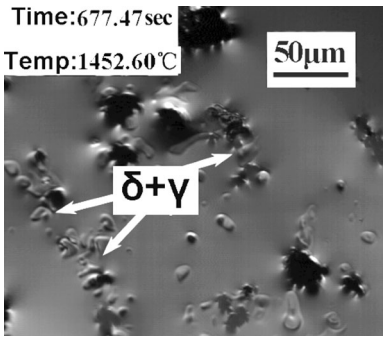

Fig. 13 In situ observation of coupled growth microstructure of δ + γ in 316LN-2 cooled at 10 °C s^{-1}

consistent with the prediction of Hammar and Svensson equations.

(2) As the cooling rate increases in the range of 0–100 °C s^{-1}, the solidification modes of both alloys do not change on the whole. However, the ferrite in 316LN-1 changes from island-like to lacy-like and it becomes coarser in 316LN-2 with cooling rate increasing. In alloy 316LN-1, the contents of Cr and Mo decrease slightly in both δ ferrite and γ phase while Ni increases in γ phase and decreases in δ ferrite in a small scale with the increasing of cooling rate. On the other hand, Cr and Mo increase in δ ferrite and decrease in austenite, while Ni has a contrary variation trend in alloy 316LN-2.

(3) Eutectic reaction occurs in the three-phase region of 316LN-1, while peritectic reaction occurs in 316LN-2 when it is cooled at 2 °C s^{-1}. The bigger diffusivities of Cr and Ni in primary δ ferrite than that in primary austenite, as well as the positions of alloys in phase diagram were thought to be the main reasons accounting for the difference in the type of three-phase reaction. Peritectic reaction transforms into eutectic reaction in 316LN-2 when it is cooled at 10 and 100 °C s^{-1}.

Acknowledgements The authors would like to thank the National High-Tech Research and Development Program of China (863 Program) for the financial support through Grant No. 2012AA03A507. We also acknowledge Dr. Yu Liu and Dr. Jianhua Wu in the Institute of New Materials in Shandong Academy of Science for their help in carrying out CSLM experiment.

References

1. Saha S, Mukherjee M, Kumar Pal T (2015) Microstructure, texture, and mechanical property analysis of gas metal arc welded AISI 304 austenitic stainless steel. J Mater Eng Perform 24:1125–1139. doi:10.1007/s11665-014-1374-0
2. de Lima MSF, Sankaré S (2014) Microstructure and mechanical behavior of laser additive manufactured AISI 316 stainless steel stringers. Mater Des 55:526–532. doi:10.1016/j.matdes.2013.10.016
3. Amudarasan NV, Palanikumar K, Shanmugam K (2013) Mechanical properties of AISI 316L austenitic stainless steels welded by GTAW. Adv Mater Res 849:50–57. doi:10.4028/www.scientific.net/AMR.849.50
4. Plaut RL, Herrera C, Escriba M, Rios PR, Padilha AF (2007) A short review on wrought austenitic stainless steels at high temperatures: processing, microstructure, properties and performance. Mater Res 10:453–460. doi:10.1590/S1516-14392007000400021
5. Hunter A, Ferry M (2002) Phase formation during solidification of AISI 304 austenitic stainless steel. Scr Mater 46:253–258. doi:10.1016/S1359-6462(01)01215-5
6. Takalo T, Suutala N, Moisio T (1979) Austenitic solidification mode in austenitic stainless steel welds. Metall Trans A 10A:1173–1181. doi:10.1007/BF02811663
7. Brooks JA, Thompson AW (1991) Microstructural development and solidification cracking susceptibility of austenitic stainless steel welds. Int Mater Rev 36:16–44. doi:10.1179/imr.1991.36.1.16
8. Suutala N (1983) Effect of solidification conditions on the solidification mode in austenitic stainless steels. Metall Trans A 14A:191–197. doi:10.1007/BF02651615
9. Di Schino A, Mecozzi MG, Barteri M, Kenny JM (2000) Solidification mode and residual ferrite in low-Ni austenitic stainless steels. J Mater Sci 35:375–380. doi:10.1023/A:1004774130483
10. Huang FX, Wang XH, Wang WJ (2012) Microstructures of austenitic stainless steel produced by twin-roll strip caster. J Iron Steel Res Int 19:57–61. doi:10.1016/S1006-706X(12)60060-0
11. Ma JC, Yang YS, Tong WH, Fang Y, Yu Y, Hu ZQ (2007) Microstructural evolution in AISI304 stainless steel during directional solidification and subsequent solid-state transformation. Mater Sci Eng, A 444:64–68. doi:10.1016/j.msea.2006.08.039
12. Fu JW, Yang YS, Guo JJ, Ma JC, Tong WH (2009) Formation of two-phase coupled microstructure in AISI 304 stainless steel during directional solidification. J Mater Res 24:2385–2390. doi:10.1557/jmr.2009.0282
13. Fu JW, Yang YS, Guo JJ, Ma JC, Tong WH (2008) Formation of a two-phase microstructure in Fe–Cr–Ni alloy during directional solidification. J Cryst Growth 311:132–136. doi:10.1016/j.jcrysgro.2008.10.021
14. Bai L, Ma YL, Xing SQ, Liu CX, Zhang JY (2015) Phase morphology evolution in AISI301 austenite stainless steel under different cooling rates. J Wuhan Univ Technol-Mater Sci Ed 30:392–396. doi:10.1007/s11595-015-1158-x
15. Tate SB, Liu S (2014) Solidification behaviour of laser welded type 21Cr–6Ni–9Mn stainless steel. Sci Technol Weld Joi 19:310–317. doi:10.1179/1362171813Y.0000000189
16. Rajasekhar K, Harendranath CS, Raman R, Kulkarni SD (1997) Microstructural evolution during solidification of austenitic stainless steel weld metals: a color metallographic and electron microprobe analysis study. Mater Charact 38:53–65. doi:10.1016/S1044-5803(97)80024-1
17. Elmer JW, Allen SM, Eagar TW (1989) Microstructural development during solidification of stainless steel alloys. Metall Mater Trans A 20:2117–2131. doi:10.1007/BF02650298

18. Zhu ZL, Ma GJ, Yu CF (2014) In situ observation of inclusions behavior in molten state and solidifying interface of tire cord steel. Adv Mater Res 881–883:1584–1587. doi:10.4028/www.scientific.net/AMR.881-883.1584
19. Huang FX, Wang XH, Zhang JM, Ji CX, Fang Y, Yu Y (2008) In situ observation of solidification process of AISI 304 austenitic stainless steel. J Iron Steel Res Int 15:78–82. doi:10.1016/S1006-706X(08)60271-X
20. McDonald NJ, Sridhar S (2005) Observations of the advancing δ-ferrite/γ-austenite/liquid interface during the peritectic reaction. J Mater Sci 40:2411–2416. doi:10.1007/s10853-005-1967-y
21. Katayama S, Matsunawa A (1984) Solidification microstructure of laser welded stainless steels. Proc. ICALEO, pp 60–67
22. Loser W, Thiem S, Jurish M (1993) Solidification modeling of microstructures in near-net-shape casting of steels. Mater Sci Eng, A 173:323–326. doi:10.1016/0921-5093(93)90237-9
23. Baldissin D, Baricco M, Battezzati L (2007) Microstructures in rapidly solidified AISI 304 interpreted according to phase selection theory. Mater Sci Eng, A 449–451:999–1002. doi:10.1016/j.msea.2006.02.248
24. Hammar O, Svensson U (1979) Solidification and casting of metals. The Metals Society, London
25. Li JY, Sugiyama S, Yanagimoto J (2005) Microstructural evolution and flow stress of semi-solid type 304 stainless steel. J Mater Process Technol 161:396–406. doi:10.1016/j.jmatprotec.2004.07.063
26. Fu JW, Yang YS, Guo JJ, Tong WH (2008) Effect of cooling rate on solidification microstructures in AISI 304 stainless steel. Mater Sci Tech-Lond 24:941–944. doi:10.1179/174328408X295962
27. Juretzko FR, Dhindaw BK, Stefanescu DM, Sen S, Curreri PA (1998) Particle engulfment and pushing by solidifying interfaces: part 1. Ground experiments. Metall Mater Trans A 29:1691–1696. doi:10.1007/s11661-998-0091-4
28. Stefanescu DM, Catalina A (1998) Calculation of critical velocity for pushing/engulfment transition of nonmetallic inclusions in Steel. ISIJ Int 38:503–505. doi:10.2355/isijinternational.38.503
29. Liang GF, Wang CQ, Fang Y (2006) In-situ observation on movement and agglomeration of inclusion in solid-liquid mush zone during melting of stainless steel AISI304. Acta Metall Sin 42:708–714. doi:10.3321/j.issn:0412-1961.2006.07.007
30. Tsuchiya S, Ohno M, Matsuura K (2012) Transition of solidification mode and the as-cast γ grain structure in hyperperitectic carbon steels. Acta Mater 60:2927–2938. doi:10.1016/j.actamat.2012.01.056
31. Valiente Bermejo MA (2012) Influence of the [Cr_{eq} + Ni_{eq}] alloy level on the transition between solidification modes in austenitic stainless steel weld metal. Weld World 56:2–14. doi:10.1007/BF03321390
32. Moharil DB, Jin I, Purdy GR (1974) The effect of δ-ferrite formation on the post-solidification homogenization of alloy steels. Metall Trans 5:59–63. doi:10.1007/BF02642927